Regular Article

PHYSICAL CHEMISTRY RESEARCH
Published by the
Iranian Chemical Society
www.physchemres.org
info@physchemres.org

Phys. Chem. Res., Vol. 12, No. 2, 289-303, June 2024
DOI: 10.22036/pcr.2023.409956.2390

Discovery of Eugenol-derived Drug Candidates for the Treatment of COVID-19 by Applying Molecular Docking, Molecular Dynamics, and Pharmacokinetic Analysis

N. Mounadi, H. Nour, A. Errougui, M. Talbi, M. El Kouali and S. Chtita*

Laboratory of Analytical and Molecular Chemistry, Faculty of Sciences Ben M'Sik, Hassan II University of Casablanca, B. P 7955 Casablanca, Morocco

(Received 3 August 2023, Accepted 5 August 2023)

Given the pandemic of COVID-19, the new generation of coronavirus noted SARS-CoV-2 remains a global health threat to this day, the absence of effective and reliable treatments against its severe acute respiratory syndromes implies day after day forced and relentless research in order to delimit the degree of danger of this virus. In this work, we performed *in silico* studies on some Eugenol derivatives in order to suggest promising molecules that could be anti-SARS-CoV-2 drugs, in the first step, a molecular docking study was conducted on a set of 59 compounds derived from Eugenol as inhibitors of the main protease (M^{pro}) SARS-CoV-2, based on the results, six compounds (51, 10, 7, 54, 4, and 59) were distinguished by the best energy scores, have been chosen to show the binding mode of eugenol derivative inhibitors, subsequently, we proceeded to the prediction of pharmacokinetics and ADMET properties on six compounds that showed good affinity towards the main protease, only one compound noted 54, according to the selection criteria of Lipinski and Veber, showed pharmacological properties suitable for human administration. In addition, the binding stability of the selected compound with our base protein was evaluated by performing molecular dynamics (MD) simulations which consequently showed good stability with SARS-CoV-2 M^{pro} under aqueous conditions.

Keywords: Molecular docking, Covid-19, Molecular dynamic, ADMET, Eugenol

INTRODUCTION

In December 2019, in Wuhan, the world saw the day of the birth of SARS-CoV-2, the thing that caused a global pandemic posing a serious danger to global health, so the need for effective and rapid viral treatment has become a paramount need worldwide.

Until now, the number of people infected by this virus is increasing day after day, it was estimated, at the time of writing this article, 671 M cases with a number of 6,84 M deaths (http://covid19.who.in). According to the degree of the danger of the current situation, international governments and scientists have been gathering their efforts, prioritizing any kind of development of accelerated treatment in order to remedy this problem, minimize the damage and avoid the spread of this virus, however, despite their efforts, any valid drug treatment against COVID-19 is not yet available for the public. Now, there are several types of candidate vaccines against this virus, approved by the WHO, some of which are mainly made available for urgent cases.

Computational studies, such as molecular docking, QSAR, molecular dynamics, pharmacokinetic studies, and others are among the most important techniques for drug discovery, regardless of the desired activity, thanks to their efficiency, flexibility of methods, and speed, all at the lowest possible cost [1-3].

Since the start of the pandemic, several works were carried out to discover anti-SARS-CoV-2 active molecules. In one of our earlier projects, we conducted a virtual screening study to evaluate a set of 129 drugs. The results

*Corresponding author. E-mail: Samirchtita@gmail.com

were supported by virtual screening and molecular docking studies on the active target of the main protease (SARS-CoV-2) (6lu7)[4].

In fact, the structural dependence of the SARS-CoV-2 virus on these ascendants is used as an indicator for studies aimed at building a candidate model of a potential drug [5]. Indeed, the main protease (M^{pro}) as the one responsible for virus replication, is considered to be a primary target on which several SARS inhibitor models have been developed [6-14].

Thanks to the antiseptic and antiviral properties of eugenol derivatives and their various biological activities, today they are frequently used in the pharmaceutical field since they are already recognized as antimicrobial agents with antioxidant action. Several works carried out relate to the studies of the properties of these organic molecules in this respect such as eugenol or isoeugenol for example [15-17].

In this work, we propose to candidate a set of compounds derived from Eugenol as drug candidates that act as inhibitors of the M^{pro} SARS-CoV-2. For this purpose, we proceeded, in silico, to the Molecular docking, ADMET, and Molecular dynamics in order to predict the performance of these compounds and to be able to give day to promising assets suitable to be candidate drugs against SARS-CoV-2. To be specific, all the studies carried out have been focused on the crystallized active target of the SARS-CoV-2 Mpro protein (noted according to PDB: 6lu7) [18].

MATERIAL AND METHODS

The database on which we based our study as candidate inhibitors of SARS-CoV-2 M^{pro}, is grouped in the form of 59 compounds derived from Eugenol, from a succession of published works (Table 1 and Table S1) [19-40].

In the first step, to perform molecular docking, we proceeded to optimize its structures using "Discovery Studio 2021" [41].

The pharmacokinetic properties of the compounds that showed good affinity towards our studied protein (M^{pro},) noted ligands, were evaluated using pkCSM-pharmacokinetics [42]. PkCSM pharmacokinetics is a tool by means of which one could predict, evaluate the ADMET properties and the ability of the studied compounds to be drug candidates.

The stability study of the studied compounds having shown good results will be supported by a simulation of molecular dynamics (MD) in order to validate our approach from upstream to downstream.

Virtual Screening of Ligand-protein Targets

Molecular docking is frequently used today because of its reliability in predicting binding, conformational style, and different types of ligand interactions at the receptor binding site.

The structure of the SARS-CoV-2 protein linked to the "N3 inhibitor" was taken from the Protein Data Bank (PDB ID: 6lu7) to perform molecular docking on its active site using a set of 59 eugenol derivatives.

Preparation of the protein and ligands. The preparation of the protein, first of all, was initiated by eliminating all the water molecules and the reference ligand "N3 inhibitor " pre-downloaded using "Discovery Studio 2021", and any other non-protein elements, the procedure is followed by adding hydrogen atoms and then Kollman charges atoms using AutoDockTools-1.5.7 [43].

Once the protein was prepared, we proceeded, before initiating molecular docking, to prime the ligands while optimizing their structures and adding hydrogen atoms. Using Avogadro software, ligand structures were optimized by means of the descent method, under the MMFF94 force field.

The parameters of the interaction site to be studied were taken as follows: The dimensions of the 3D grid box were (30 × 30 × 30) Angstrom, with the coordinates of x = -10.729, y = 12.417, z = 68.816, in accordance with the active site of our reference ligand "N3 inhibitor ".

Molecular docking of Eugenol derivatives with the SARS-CoV-2 protein (M^{pro}). After preparing the ligands for our eugenol data study, the next step is to carry out molecular docking on the target site of SARS-COV-2 M^{pro}, the objective being to evaluate their behavior, i.e. the type of interaction and affinity. The results obtained were estimated according to the value of the binding energy, namely, the lowest is judged to be the best score and consequently, it corresponds to the best molecule which interacts well with the protein site.

For those who showed the best score, we used "Discovery Studio 2021" to illustrate the type of interaction and the

Table 1. IUPAC Names of the Eugenol Derivatives Studied

N	Name	N	Name
1	Eugenol	31	4-((2,2-dimethyl-1,3-dioxolan-4-yl)methyl)-2-methoxyphenol
2	Acetyleugenol	32	4-(2-hydroxy-3-(2-hydroxyphenoxy)propyl)-2-methoxyphenol
3	4-allyl-2-methoxyphenyl benzoate	33	4-(2-hydroxy-3-(3-hydroxyphenoxy)propyl)-2-methoxyphenol
4	4-(5-allyl-3-methoxy-2-phenooxybenzyl)morpholine	34	4-(2-hydroxy-3-(4-hydroxyphenoxy)propyl)-2-methoxyphenol
5	4-allyl-2-methoxy-6(morpholinomethyl)phenol	35	5-(4-hydroxy-3-methoxybenzyl)dihydrofuran-2(3H)-one
6	4-(5-allyl-2,3-dimethoxybenzyl)morpholine	36	4-(4-hydroxy-3-methoxyphenyl)butanal
7	4-(5-allyl-2-(4-chlorophenoxy)-3-methoxybenzyl)morpholine	37	3-(4-hydroxy-3-methoxyphenyl)-2-methylpropanal
8	(2R, 4R, 5R)-2-(acetoxymethyl)-6-(4-allyl-2-methoxyphenoxy) -tetrahydro-2H-pyran-3,4,5triacetate	38	2-methoxy-4-(3-(phenylthio)propyl)phenol
9	(3R, 4R, 6R)-2-(4-allyl-2-methoxyphenoxy) -6-(hydroxymethyl)tetrahydro-2H-pyran-3,4,5-triol	39	2-((4-allyl-2-methoxyphenoxy)methyl)oxirane
10	(4aR,7R,8S,8aS)-6-(4-allyl-2-methoxyphenoxy) -2-phenylhexanhydropyrano[3,2-d][1,3]dioxine-7,8-diol	40	1-(4-allyl-2-methoxyphenoxy)-3-(diethylamino)propan-2-ol
11	4-allyl-2-methoxyphenyl 2-fluorobenzoate	41	4-allyl-2-methoxyphenyl phenylmethanesulfonate
12	4-allyl-2-methoxyphenyl 3-bromobenzoate	42	2-(4-allyl-2-methoxyphenoxy)acetic acid
13	4-allyl-2-methoxyphenyl 3-chlorobenzoate	43	methyl 2-(4-allyl-2-methoxyphenoxy)acetate
14	4-allyl-2-methoxyphenyl-4-methoxybenzoate	44	2-(4-allyl-2-methoxyphenoxy)-N,N-bis(2-hydroxyethyl)acetamide
15	4-allyl-2-methoxyphenyl 4-methylbenzoate	45	4-allyl-2-methoxy-6-nitrophenol
16	4-allyl-2-methoxyphenyl 2-phenylacetate	46	5-allyl-3-nitrobenzene-1,2-diol
17	5-allyl-7-methoxy-2-phenylbenzo[d]oxazole	47	4-allyl-2-methoxy-3-nitrophenol
18	5-allyl-7-methoxy-2-(4-methoxyphenyl)benzo[d]oxazole	48	4-allyl-4-hydroperoxy-2-methoxycyclohexa-2,5-dien-1-one
19	Iso-eugenol	49	4-allyl-2-amino-6-methoxyphenol
20	Chavicol	50	(6-(4-hydroxy-3-methoxybenzyl)-3-methyl-2,4-diazabicyclo[3.2.0]hept-3-en-2-yl)(2R)-3-(2-hydroxynaphthalen-1-yl)oxiran-2-yl)methanone
21	Chavibetol	51	5-allyl-7-methoxybenzo[d]oxazole-2(3H)-thione
22	Estragol	52	6-allyl-8-methoxy-3-methyl-3,4-dihydro-2H-benzo[e][1,3]oxazine
23	Anethol	53	6-allyl-3-(furan-2-ylmethyl)-8-methoxy-3,4-dihydro-2H-benzo[e][1,3]oxazine
24	Safrole	54	2,2'-((5,5'-diallyl-3,3'-dimethoxy-[1,1'biphenyl]-2,2'-diyl)bis(oxy)bis(ethan-1-ol)
25	Isosafrole	55	2,2'-((5,5'-di(1λ²,2 λ³,3 λ²-allyl)-3,3'-di(λ¹-methoxy)-4 λ³,4' λ³,6λ³,6'λ³ -[1,1'-bi(cyclohexane)]-1,1',3,3',5,5'-hexaene-2,2'-diyl)bis(oxy))bis(1 λ²,2 λ²-ethan-1-ol)
26	Myristicine	56	2-[(2-methoxy-4-prop-2-enylphenoxy)methyl]-3,5,6-trimethylpyrazine
27	Elemicine	57	7-chloro-4-(2-methoxy-4-prop-2-enylphenoxy)quinoline
28	Methyleugenol	58	2-((3-(λ1-methyl)-1 λ2,2 λ3,4 λ1-but-2-en-1-yl)oxy)-6-(3-(4-((3-(λ1-methyl) -1 λ2,2 λ3,4 λ1-but-2-en-1-yl)oxy)-3-(11-methoxy)-2 λ3,5 λ3,6 λ3-phenyl) -1 λ2,2 λ3,3 λ3-allyl)-3-(λ1-methoxy)-4 λ3,5 λ3-phenol
29	4-(2-hydroxypropyl)-2-methoxyphenol	59	2-(4-(1 λ2,2 λ3,3 λ2-allyl)-2-(λ1-methoxy)-3 λ3,5 λ3,6 λ3-phenoxy) -1-(3-(4-chloro-2 λ3,3 λ3,5 λ3,6 λ3-phenyl)-5-(4-hydroxy-2 λ3,3 λ3,5 λ3,6 λ3-phenyl) -2 λ2,3 λ3,4 λ2,5 λ3-pyrazolidin-1-yl)-2 λ2-ethan-1-one
30	3-(4-hydroxy-3-methoxyphenyl)propane-1,2-diol		

amino acids interacted of our target protein with the studied ligands.

ADMET Analysis of the Best Drug Candidates

In order to procure drug candidates from this work, the study of pharmacokinetic properties was done for compounds that showed promising affinity results based on molecular docking. This step must respect certain well-defined criteria according to the drug discovery process, the similarity properties of the drug (Lipinski's rule and bioavailability, veber, *etc*.). On the whole, the process which gives good stability with the least cost is considerable criteria in order to adopt a drug whatever it is. In this study, the pkCSM-pharmacokinetics web server was employed for the ADMET properties evaluation of studied molecules.

Molecular Dynamics Simulations

To highlight the nature of the 6lu7 complex formed with the best-selected eugenol compound (*i.e*., the candidate with the highest energy score in Molecular Docking with admissible pharmacokinetic properties), a molecular dynamics simulation study was carried out using GROMACS [44], under the charmm27 force field [45]. The topologies of the selected drug ligands were issued from the SwissParam server [46]. Moreover, the 6lu7-drug complexes were placed in a cubically-shaped simulation box, followed by solvation

with TIP3P water molecules and the addition of sodium and chlorine ions to condition and neutralize the entire system. After that, System optimization has been carried out by minimizing the steepest descent so as to avoid steric collisions as much as possible. Then, using the Parrinello-Rahman barostat with 1 atm for 1 ns, we first carried out NVT equilibration at 300 K for 1 ns, followed by NPT equilibration [47], the aim of which is to be able to stabilize the systems under the conditions we desire. In the end, the submission of the equilibrated system to MD for 100 ns was launched.

RESULTS AND DISCUSSIONS

Molecular Docking

Using AutoDock Vina software, the 59 Eugenol-derived compounds were taken in this study to predict their binding energy and the most possible modes of interaction with the SARS-CoV-2 M^{pro} active site. The binding energy scores obtained from the molecular docking of all compounds studied with SARS-CoV-2 M^{pro} active site are reported in Table 2.

Based on the results, six compounds (51, 10, 7, 54, 4, and 59) were found to have the highest binding energies, so they are selected to describe the binding mode of eugenol derivative candidates. Among the six chosen compounds, compound 51 was by far the most outstanding with respect to binding energy with -8.0 Kcal mol^{-1}.

Before being able to interpret the results obtained, we performed the molecular docking, in the same way and under the same conditions, of our target M^{pro} with the ligand N3 as a reference inhibitor. On the one hand, the re-docking process was applied to validate the docking protocol. As shown in Fig. 1, the re-docked structure of N3 is highly superimposed

Table 2. Predicted Binding Energies of 59 Eugenol Derivatives Anchored with 6lu7

Compound No.	BE (kcal mol^{-1})	Compound No.	BE (kcal mol^{-1})	Compound No.	BE (kcal mol^{-1})
1	-4.9	21	-4.5	41	-5.4
2	-5.4	22	-4.9	42	-6.5
3	-6.4	23	-4.5	43	-5.9
4	-7.0	24	-4.5	44	-5.7
5	-6.2	25	-5.0	45	-5.8
6	-6.2	26	-5.1	46	-5.7
7	-7.3	27	-5.3	47	-5.9
8	-6.5	28	-4.8	48	-5.4
9	-6.8	29	-4.8	49	-5.5
10	-7.4	30	-5.4	50	-5.3
11	-6.0	31	-5.4	51	-8.0
12	-6.7	32	-6.3	52	-5.5
13	-6.3	33	-6.6	53	-5.8
14	-6.3	34	-6.8	54	-7.1
15	-6.0	35	-6.7	55	-5.9
16	-6.1	36	-6.1	56	-6.7
17	-5.9	37	-5.3	57	-6.8
18	-6.9	38	-5.3	58	-6.8
19	-6.8	39	-6.0	59	-7.0
20	-5.2	40	-5.7		

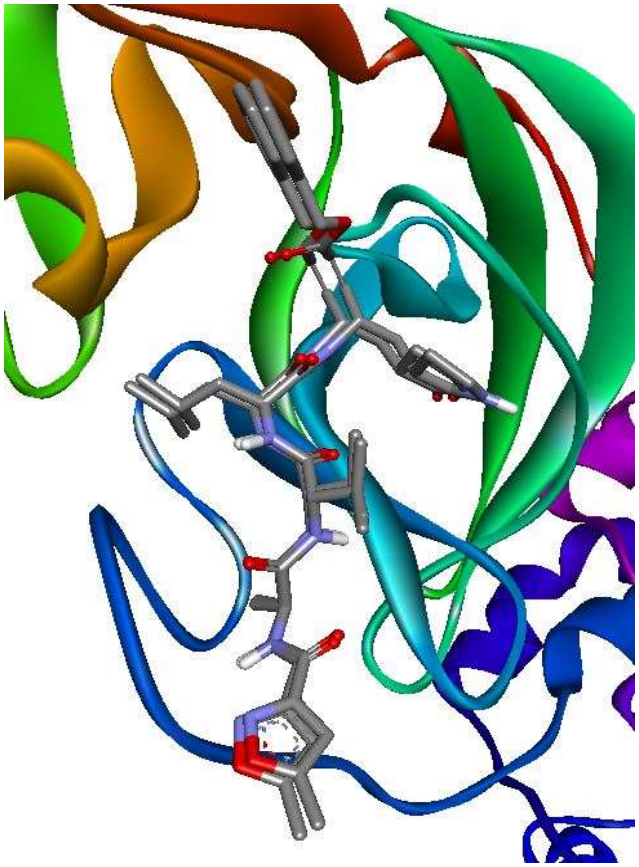

Fig. 1. The superimposition of the original and re-docked N3 at the binding site of 6lu7.

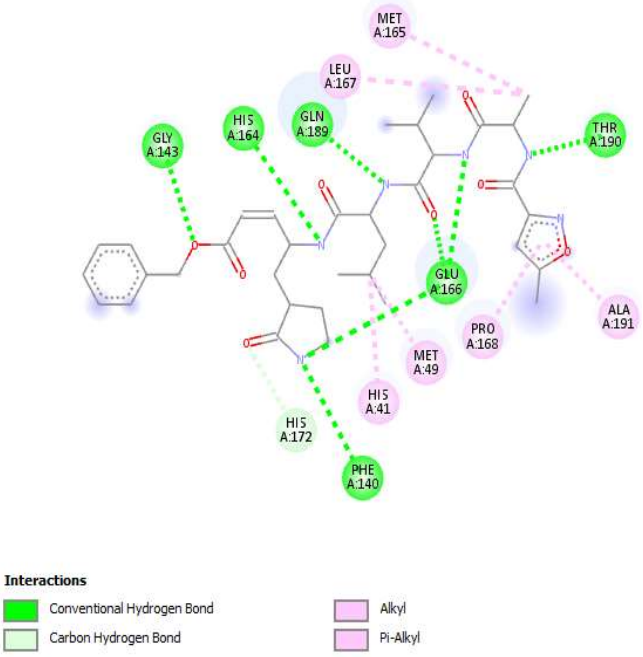

Fig. 2. Different interactions and key residues between 6lu7 and N3 inhibitor.

with its original coordinates, indicating that the docking protocol is valid. On the other hand, this is done to predict the types of residues involved in the interactions between M^{pro} and the N3 ligand, to know if the same amino acids that interacted with N3 are precisely those of our six selected compounds.

From the results obtained by comparing those of the residues interacted with the studied compounds and N3 (Figs. 2 and 3), it can be seen that there is a variety of amino acids interacted commonly at the level of all the studied compounds that showed a good score at the molecular docking and the reference inhibitory ligand N3. The thing that proves the validity of our studied model, we quote pertinently the compound 51 that represents the most important affinity (GLY143, GLU166, MET165, and LEU167 with several interactions) and the compound 54 (with GLU166, PRO168, MET165, LEU167, and PRO168).

Given the results obtained by the molecular docking of all the compounds used on the M^{pro} protein, the interactions for the ligands that showed good affinity towards our target protein were illustrated in Fig. 3, obtained for the best poses related to the pre-selected ligands.

Figure 3 and Table 3 illustrate the amino acids in the M^{pro} protein that interact with the ligands, as a whole, there are favorable interactions type Van der Walls, hydrophobic interactions (Pi-Pi T-shaped, Amide-Pi Stacked, Alkyl, Pi-Alkyl), hydrogen bonds (hydrogen bond, C-H), electrostatic (Pi-cation ...).

The results show that compound No. 51 is the most promising as an inhibitory ligand for (M^{pro},) SARS-CoV-2 protein, in addition to its estimated binding energy of -8.0 Kcal mol^{-1}, compound 51 is found to be capable of forming various favorable interactions, 5 hydrogen bonds with different amino acids (4 conventional hydrogen bonds with GLY143, SER144, and CYS145 at 2.482, 1.953, 2.977, 3.756 Å respectively and another C-H type with GLU166 at 3.582 Å); 2 hydrophobic bonds (Alkyl type with MET165 and LEU167 respectively at 4.296 and 5.119 Å) and other Pi-Sulfur type with MET165 at 5.935 Å (Fig. 3: 51(D)).

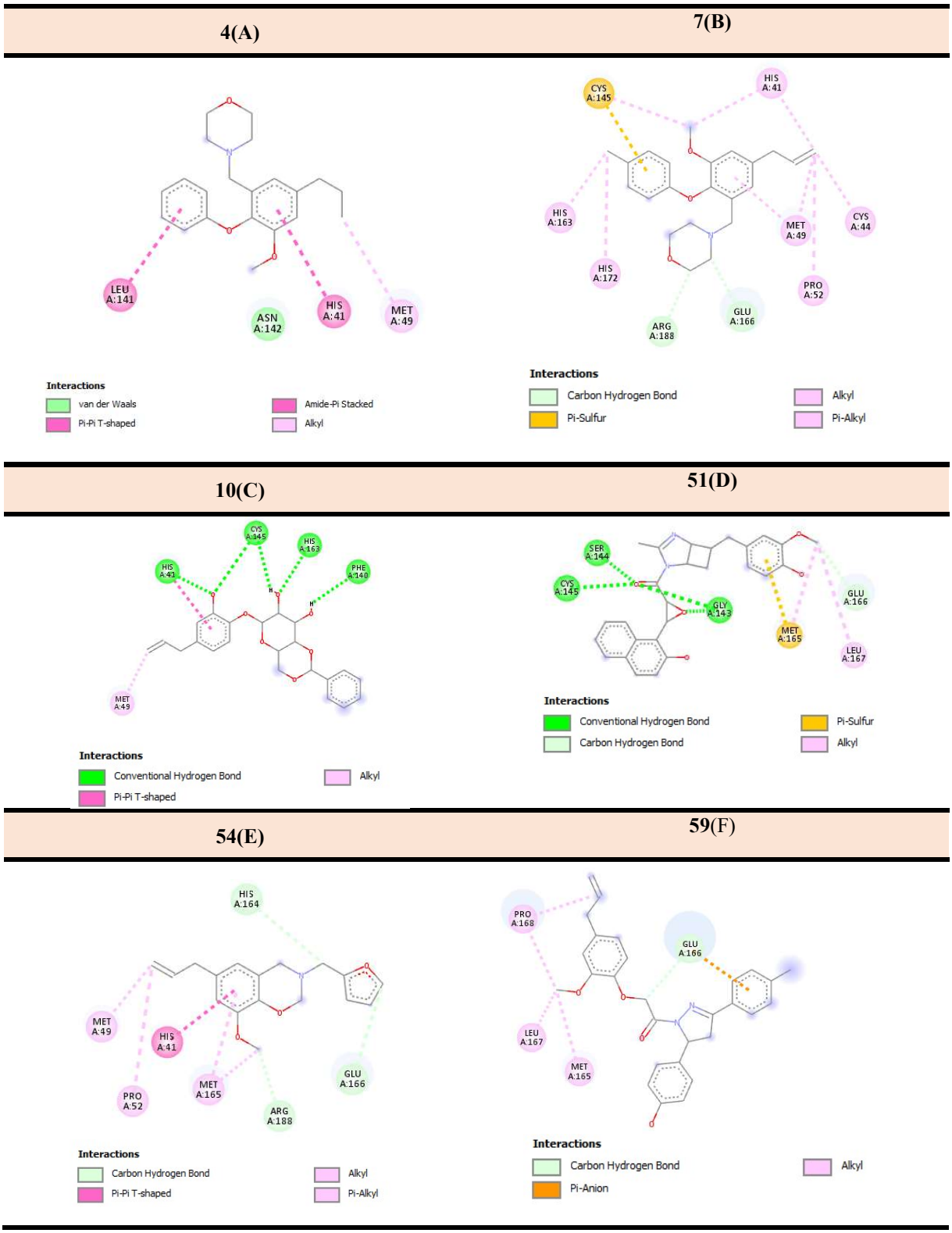

Fig. 3. Illustrations of type of interactions between amino acids of protein 6lu7 with compounds (A) 4, (B) 7, (C) 10, (D) 51, (E) 54, and (F) 59.

Table 3. Type of Interactions between Amino Acids (Residues) of Protein 6lu7 with Compounds 51, 10, 7, 54, 4 and 59

Compound	Residues	Distance	Interaction type	Compound	Residues	Distance	Interaction type
4	HIS41	5.410	Pi-Pi T-shaped (Hydroph)	51	GLY143	2.483	Conventional Hydrogen Bond
	LEU141	4.741	Amide-Pi Stacked (Hydroph)		GLY143	1.953	
	ASN142-MET49	4.119	Alkyl (Hydroph)		SER144	2.978	
7	GLU166	3.472	Carbon Hydrogen Bond		CYS145	3.757	
	ARG188	3.606			GLU166	3.583	Carbon Hydrogen Bond
	CYS145	5.244	Pi-Sulfur		MET165	5.936	Pi-Sulfur
	CYS44	4.558	Alkyl (Hydroph)		MET165	4.296	Alkyl
	MET49	3.735			LEU167	5.120	Alkyl
	PRO52	4.875		54	ARG188	3.734	Carbon Hydrogen Bond
	CYS145	4.230			HIS164	3.656	
	HIS41	5.170	Pi-Alkyl (Hydroph)		GLU166	3.573	
	HIS41	4.421			HIS41	5.246	Pi-Pi T-shaped (Hydroph)
	HIS163	4.569			MET49	3.977	Alkyl (Hydroph)
	HIS172	4.629			PRO52	4.895	
	MET49	5.054	Pi-Alkyl		MET165	4.253	
10	HIS41	2.628	Conventional Hydrogen Bond		MET165	4.952	Pi-Alkyl (Hydroph)
	CYS145	3.612		59	GLU166	3.628	Carbon Hydrogen Bond
	HIS163	2.598			GLU166	3.260	Pi-Anion (Electrostatic)
	PHE140	2.753			PRO168	4.034	Alkyl (Hydroph)
	CYS145	2.947			MET165	4.868	
	HIS41	4.900	Pi-Pi T-shaped (Hydroph)		LEU167	4.558	
	MET49	3.975	Alkyl (Hydroph)		PRO168	4.801	

We find in 2nd classification the compound No. 10, with a binding energy estimated at -7.4 Kcal mol^{-1}, the binding capacity of this ligand is also favorable, with 5 hydrogen bonds formed with different amino acids of M^{pro} (HIS41, CYS145, HIS163, PHE140, and CYS145 respectively at a distance of 2, 628, 3.612, 2.597, 2.753, 2.946 Å), 2 hydrophobic interactions (one Pi-Pi T-shaped type with HIS41, the 2nd alkyl type with MET49, respectively with a distance of 4.899and 3.975 Å (Fig. 3: 10(C)).

Compound No.7 also has an affinity towards the protein M^{pro}, while forming favorable bonds such as hydrogen, it is thus associated with two H-bonds formed as C-H with the amino acids of GLU166 and ARG188 respectively with a distance of 3.472 and 3.606 Å. The docking score for the best interaction is -7.40 Kcal mol^{-1}. The conformational energy of the ligand was minimized by the presence of 10 hydrophobic interactions (one Pi-Sulfur with CYS145 at5.244 Å and 4 alkyl with CYS44, MET49, PRO52, CYS145 at 4.557, 3.735, 4.874, 4, 229 Å and 5 Pi-Alkyl with HIS41, HIS163, HIS172, and MET49 at 5.170, 4.421, 4.569, 4.629, 5.052 Å respectively) which translates into a charge transfer involved in intercalating the ligand into the 6lu7 binding target.

Compound no. 54 gave a molecular docking score of -7.10 Kcal mol^{-1} for the best-predicted pose, with 3 hydrogen bonds formed with ARG188, HIS164, and GLU166 at 3.733, 3.655, 3.572 Å respectively, The energy of the ligand is minimized by the abundance of 5 hydrophobic interactions (one Pi-Pi T-shaped with HIS41 at 5.245 Å, 3 alkyl type with MET49, PRO52, and MET165 respectively at 3.976, 4.89468 and 4.252 Å and finally one Pi-Alkyl type with MET165 at 4.952 Å).

Compounds No. 59 and 4 come last in the selection with equal docking scores of -7.00 Kcal mol^{-1}. Compound No. 59 shows favorable interactions with the studied protein including a hydrogen bond of C-H nature with GLU166 at 3.6276 Å and other hydrophobic type alkyl with PRO168, MET165, LEU167, and PRO168 respectively at 3.259, 4.033, 4.867, 4.557 and 4.800 Å and a Pi-Anion electrostatic interaction with GLU166 at 3.25976 Å. On the other hand, Compound 4 forms only hydrophobic bonds: a Pi-Pi T-shaped with HIS41 at 5.410 Å and an Amide-Pi Stacked with LEU141 and ASN142 at 4.741 Å, an alkyl type with MET49 at 4.119 Å, Van Deer Walls interactions are also present with ASN142 which allows improving the affinity of the

compound towards the M^{pro} (Fig. 3: 4(A)).

Prediction of Pharmacokinetics (ADMET)

In order to be able to find candidate molecules as innovative drugs in such a fast and reliable way and by minimizing the time that it is necessary to debit to the laboratory and to the experimental studies which prove to be expensive, the use of the data-processing methods to develop this concept is really paramount as long as they answer well the desired expectations. For this purpose, we used the online pkCSM as a tool to calculate the ADMET properties as a measure of pharmacokinetics.

To be able to study the Pharmacokinetics and the prediction of the similarity of drugs for the 6 compounds studied previously (N°51, 10, 7, 54, 4, and 59), There are several rules and methods of selection of molecules as drugs, among them, we quote the most relevant: Lipinski's rules otherwise known as the rule of 5, as well as Veber's rules.

The study of molecular docking already carried out remains only a preliminary and indicative selection to move to this stage and therefore does not allow to be used only for the development of drugs.

As for Lipinski's rules, the pharmacologically active molecules to be selected must have an acceptable bioavailability with good oral absorption, so the molecular weight must be (Mw < 500), logP < 5, hydrogen bond donor groups (HBD < 5) and hydrogen bond acceptor groups (HBA < 10). If no more than two parameters exceed this rule, poor absorption or permeability will be possible [48]. Veber's rule is proportional to the number of rotating bonds which must be (RB) ≤ 10 and the polar area which has a proportional relationship with absorption properties in drug discovery process studies ((PSA) ≤ 140) [49].

Lipinski and Veber selections. First, we will examine the parameters given by the pkCSM for each selected compound using the Lipinski and Veber rules in order to study the acceptability of these compounds to be drug candidates

According to Table 4, compounds 51, 10, 7, 54, and 4 perfectly meet the criteria given by Lipinski and therefore there will be no bioavailability problems with them. Compound 59 even if (logP) exceeds 5 remains included in the selection of acceptability according to Lipinski.

In addition, as for Veber's rule, all the studied compounds except N°54 are unacceptable, their polar surface far exceeds 140, one could say that these compounds have a strong polarity and consequently, they will not be easily absorbed by the membranes that differs for the case of the compound 54 which has a PSA = 124.129 lower than 140, namely an acceptable solubility and good accessibility through protein membranes.

The number of RB rotational bonds is an indicator of the flexibility of the molecules and their ability to be accessible for particular interactions with the desired target. In this case, all the studied compounds meet Veber's rules for the number of rotational bonds with (RB) ≤ 10.

In conclusion, Veber's rule-based selection of potential candidates allowed us to select only compound 54 that meets the drug similarity evaluation criteria, while the other compounds are rejected due to violation of a Veber criterion (Table 4).

Evaluation of ADMET properties. Absorption: The

Table 4. Prediction of Lipinski & Veber Parameters for the Six Main Compounds

Compound N°	Lipinski				Veber	
	Mw ($g\ mol^{-1}$)	LogP	HBA	HBD	Surface area	RB
4	341.451	4.272	4	0	149.868	7
7	373.880	4.702	4	0	159.481	7
10	400.427	2.060	7	3	168.274	5
51	460.530	3.477	6	3	197.454	5
54	285.343	3.369	4	0	124.129	5
59	478.976	5.381	5	2	203.901	8

importance of this step during the administration of drugs is paramount because a drug will not be so if it would have a problem of absorption. Whatever the route of administration of the drug, once consumed, it disintegrates into the active molecule and therefore enters the systemic circulation. There are several factors influencing the absorption of substances, such as solubility, permeability, and surface area [50].

From the results obtained in Table 5, especially for compound 54 since it was admitted according to the selection of Veber and Lipinski, all compounds showed acceptable values (logSwat (> -5.7)), so it can be concluded that they have good water solubility.

Since logPapp must be greater than 0.9, compound 54 (logPapp = 1.818) is therefore considered to be fairly permeable *via* Caca2.

In order for the compounds studied to be absorbed in the intestines, the absorbance should be higher than 30%. According to the results, all the tested compounds exceed 30% by far.

Skin permeability is still an essential factor in improving the efficacy of drugs, especially in the development of transdermal drugs. It is considered that there is a difficulty of penetration of molecules into the skin if logKp is higher than -2.5 cm h^{-1}. From Table 5, it can be seen that all the evaluated compounds have a good skin permeability (lower than -2.5 cm h^{-1}).

Distribution: According to Table 5, the predicted VDss of the different compounds, except number 10, is higher than the optimal value (> 0.45); so we can conclude that the drug in large part will be in the tissues rather than binding to blood plasma. Compounds cross the blood-brain barrier without any problem if the logBB would be greater than 0.3, whereas compounds with logBB < -1 will be considered poorly distributed to the brain. The logBB is greater than -1, that is, there will be no problem in their distribution to the brain. In addition, the compounds with LogPS > -2 have the ability to

Table 5. Evaluation of ADMET Parameters Predicted by PKCSM

Property	Model name	4	7	10	51	54	59	Unit
Absorption	Water solubility	-3.697	-3.85	-3.72	-3.439	-2.484	-5.531	**Numeric** (log mol/L)
	Caco2 permeability	0.838	0.837	0.639	0.592	1.818	0.571	(log Papp in 10^{-6} cm/s)
	Intestinal absorption (human)	88.969	87.784	73.313	88.441	91.664	87.86	(% Absorbed)
	Skin Permeability	-2.667	-2.671	-2.744	-2.735	-2.512	-2.748	(log Kp)
	P-glycoprotein substrate	Yes	Yes	Yes	Yes	Yes	Yes	**Categorical** (Yes/No)
	P-glycoprotein I inhibitor	Yes	Yes	No	Yes	No	Yes	
	P-glycoprotein II inhibitor	Yes	Yes	No	Yes	No	Yes	
Distribution	VDss (human)	1.511	1.473	-0.129	1.143	0.856	-0.108	**Numeric** (log L/kg)
	Fraction unbound (human)	0.214	0.2	0.063	0.024	0.419	0	**Numeric** (Fu)
	BBB permeability	0.909	0.877	-0.704	-0.716	0.519	-0.134	(log BB)
	CNS permeability	-1.828	-1.814	-3.176	-2.445	-1.922	-1.974	(log PS)
Metabolism	CYP2D6 substrate	No	No	No	No	No	No	**Categorical** (Yes/No)
	CYP3A4 substrate	Yes	Yes	No	Yes	No	Yes	
	CYP1A2 inhibitior	Yes	Yes	No	No	Yes	No	
	CYP2C19 inhibitior	Yes	Yes	No	Yes	Yes	Yes	
	CYP2C9 inhibitior	No	No	No	Yes	No	Yes	
	CYP2D6 inhibitior	Yes	Yes	No	Yes	Yes	No	
	CYP3A4 inhibitior	No	No	No	Yes	No	Yes	
Excretion	Total Clearance	1.013	1.03	0.956	0.813	1.156	-0.104	**Numeric** (log ml/min/kg)
	Renal OCT2 substrate	No	No	No	No	Yes	No	**Categorical** (Yes/No)
Toxicity	AMES toxicity	Yes	No	No	No	No	No	**Categorical** (Yes/No)
	Max. tolerated dose (human)	0.441	0.424	-0.394	-0.282	-0.137	0.132	**Numeric** (log mg/kg/day)
	hERG I inhibitor	Yes	Yes	No	No	No	No	**Categorical** (Yes/No)
	hERG II inhibitor	Yes	Yes	No	Yes	Yes	Yes	
	Oral Rat Acute Toxicity (LD50)	3.154	3.229	2.11	2.621	3.321	2.193	**Numeric** (mol/kg)
	Oral Rat Chronic Toxicity (LOAEL)	0.756	1.315	2.459	1.2é44	1.451	2.21	
	Hepatotoxicity	Yes	No	No	Yes	No	Yes	
	Skin Sensitisation	No	No	No	No	No	No	**Categorical** (Yes/No)
	T.Pyriformis toxicity	0.295	0.295	0.285	0.286	0.464	0.387	**Numeric** (log ug/L)
	Minnow toxicity	-0.547	-0.782	1.266	2.11	1.278	-2.225	(log mM)

easily access the central nervous system (CNS) while logPS < -3 shows the inability of these compounds to penetrate the CNS. According to these results, only compound 10 is recognized to be unable to penetrate the CNS.

Metabolism: The prediction of metabolism is carried out on the basis of CYP models (CYP2C19 CYP2D6, CYP3A4, CYP1A2, and CYP2C9). Table 5 illustrates that compound 10 neither affects nor inhibits all enzymes. Therefore, there will be no constraint for it to be metabolized in the liver, on the other hand, the other compounds differ in terms of behavior towards the model CYP enzymes.

Excretion: The prediction of the total clearance of a compound is given by log(CLtot) in log(ml/min/kg). When the compound's estimated CLtot value is predicted to be high, we can deduce that excretion will be rapid Toxicity

The toxicity results of the eugenol-derived compounds studied are detailed in Table 5. The LD50 value is expressed as an indication to evaluate the toxicity of the tested compounds according to their dose, *i.e.* the higher it is (in this case LD50 varies from 2.11 to 3.321) *i.e.* the compounds studied are lethal only at extremely high doses. A compound is said to be potentially mutagenic if the AMES test result is found to be positive, based on the results only compound 4 is predicted to be mutagenic. The results also show that none of the tested compounds caused skin sensitization.

Molecular Dynamics Simulations

The dynamic simulation of 6lu7 and its complex with compound 54 was carried out during 100 ns, to gain insight into their stability in an aqueous environment. Figures 4 to 8 present the trajectories of the parameters calculated during the performed simulations, namely, root mean square deviations analysis (RMSD), root means square fluctuation analysis (RMSF), the radius of gyration (RoG), several hydrogen bonds (H-bond) and solvent accessible surface area (SASA).

According to Figure 4, RMSD of the 6lu7 and 6lu7-compound 54 complex fluctuates until it stabilizes after 40 ns. Moreover, the values of their RMSD don't exceed 0.4 nm throughout the simulation. Nevertheless, the trajectory of RMSD corresponding to the 6lu7-L164 complex exhibited more fluctuations compared to the 6lu7-compound 54 complex. In addition, the mean RMSD values of 6lu7 and 6lu7-compound 54 proved to be 0.219 nm and 0.269 nm, respectively. We also note that the RMSD trajectory of the 6lu7- compound54 complex is like that of 6lu7, indicating that compound 54 does not induce any significant structural changes distorting the three-dimensional structure of 6lu7. Overall, the obtained results highlight that the molecular recognition of compounds 54 and 6lu7 leads to a stable complex.

Besides, as depicted in Fig. 5, the RMSF trajectory corresponding to 6lu7-compound 54 is relatively comparable to that of 6lu7, exhibiting that compound 154 induces no potential conformational changes on 6lu7. In addition, the mean RMSF values of 6lu7 and 6lu7-compound 54 were 0.102 and 0.129 nm, respectively. Furthermore, several residues of 6lu7 complexed with compound 54 were found to have low RMSF values, indicating the stability of the 6lu7-compound54 complex.

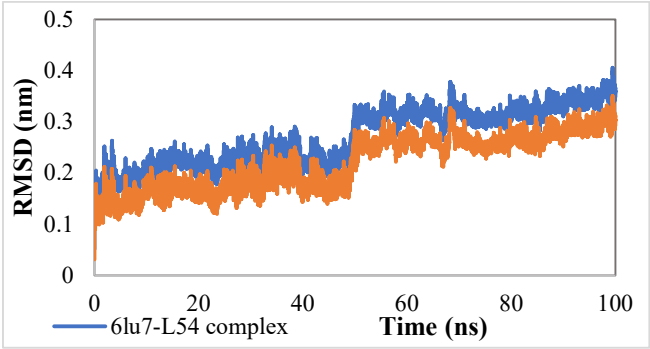

Fig. 4. RMSD of the backbone of 6lu7 uncomplexed and 6lu7- compound54 complex as a function of time.

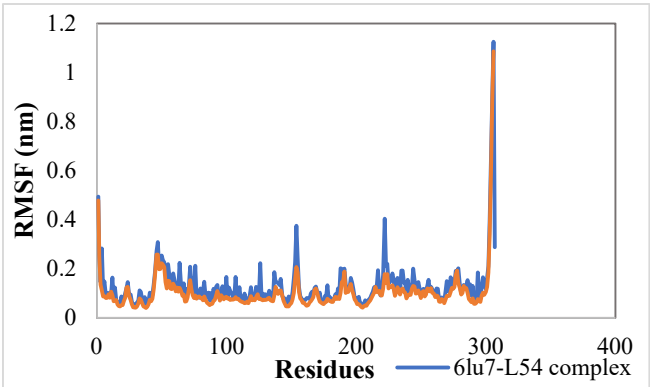

Fig. 5. RMSF of Cα atoms of 6lu7 in the absence and presence of compound 54.

Figure 6 presents the RoG trajectory of 6lu7 and its complexes. The average RoG values of 6lu7 and 6lu7-compound54 complex were calculated to be 2.243 nm and 2.241 nm, respectively. Besides, the RoG trajectory relative to 6lu7- compound 54 was relatively steady during the entire simulation, supporting the stability of the 6lu7-compound54 **complex in an aqueous environment.**

Figure 7 presents the trajectory of the solvent-accessible surface area (SASA) corresponding to all studied systems. The mean SASA values of 6lu7 and 6lu7-compound54 complex were found to be 150.866 nm^2 and 149.720 nm^2, respectively. In addition, the SASA trajectory of 6lu7 is comparable to that of the 6lu7-compound 54 complex and they were at a steady state during the entire simulation, indicating that the 6lu7 underwent no relevant conformational change during its molecular recognition with compound 54. Besides, as depicted in Fig. 8, compound 54 may have involved a large number of hydrogen bonds with its receptor, supporting its stability in the aqueous medium.

MM-GBSA Analysis

The binding free energy of the 54-6lu7 complex in aqueous medium was calculated by applying MM-GBSA. The calculation was performed using the last 252 complex frames. As presented in Table 6, -18.27 Kcal mol^{-1} is the binding energy found, which means that the ligand-protein recognition was favorable, which confirms the docking results. Furthermore, the Van der Waals interactions are highly favorable for ligand-protein binding.

Overall, according to MD and MM-GBSA results, the molecular recognition between compounds 54 and 6lu7 lead to favorable and stable complexes.

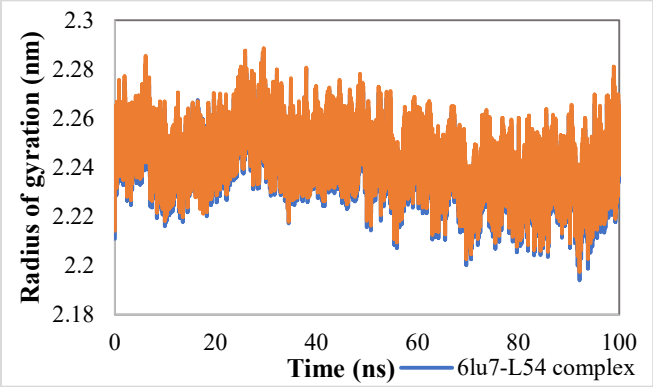

Fig. 6. (a) RoG of 6lu7 and 6lu7-L154 complex as a function of time.

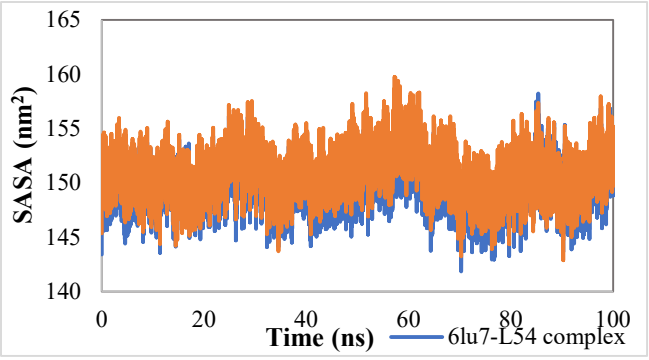

Fig. 7. The solvent accessible surface area (SASA) of 6lu7 and it's complex with compound 54.

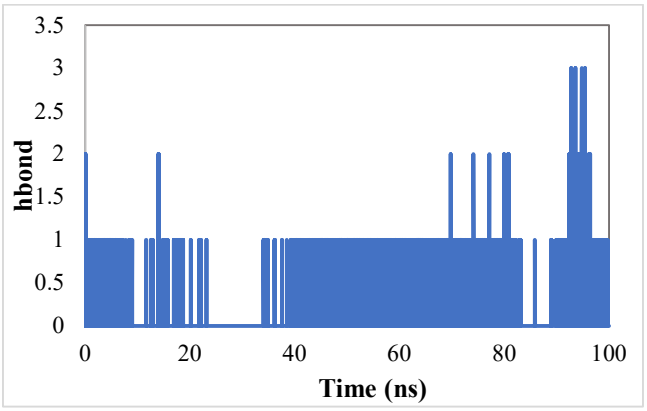

Fig. 8. The number of hydrogen bonds involved 6lu7 and the compound 54 as a function of time.

Table 6. MM-GBSA Calculation for Binding Free Energy (Kcal mol^{-1})

Energy component	Value
ΔE_{VDW}	-36.06
ΔE_{ELEC}	-5.07
ΔG_{POLAR}	23.30
$\Delta G_{NON-POLAR}$	-4.60
$-T\Delta S$	4.17
$\Delta G_{BINDING}$	-18.27

CONCLUSION

After having performed the molecular docking on a set of 59 eugenol-derived compounds, six compounds showed promoter interactions with the main protease protein, subsequently, according to the selection criteria of Lipinski and Veber only compound 54 has been selected, therefore it seems that this compound is acceptable for oral administration, its ADMET properties are more or less acceptable. In addition, the dynamic simulation study of this compound with SARS-CoV-2 Mpro under aqueous conditions has shown good stability. Consequently, Further validation is required, such as in vivo and in vitro studies to predict whether our compound 54 is a good drug candidate against SARS-CoV-2.

REFERENCES

[1] Ghosh, S.; Mali, S. N.; Bhowmick D. N.; Pratap, A. P., Neem oil as natural pesticide: Pseudo ternary diagram and computational study. *J. Indian* Chem. Soc. **2021**, *98* (7), 100088, DOI: https://doi.org/10.1016/j.jics.2021.100088.

[2] Mali, S. N.; Pandey, A., Multiple QSAR and molecular modelling for identification of potent human adenovirus inhibitors. *J. Indian Chem. Soc.* **2021**, *98* (6), 100082, DOI: https://doi.org/10.1016/j.jics.2021.100082.

[3] Mali, S. N.; Pandey, A.; Thorat, B. R.; Lai, C. H., Multiple 3D-and 2D-quantitative structure-activity relationship models (QSAR), theoretical study and molecular modeling to identify structural requirements of imidazopyridine analogues as anti-infective agents against tuberculosis. *Struct. Chem.* **2022**, *33* (3), 679-694, DOI: https://doi.org/10.1007/s11224-022-01879-2.

[4] Chtita, S.; Belhassan, A.; Aouidate, A.; Belaidi, S.; Bouachrine, M.; Lakhlifi, T., Discovery of potent SARS-CoV-2 inhibitors from approved antiviral drugs via docking and virtual screening. *Comb. Chem. High Throughput Screen.* **2021**, *24* (3), 441-454, DOI: https://doi.org/10.2174/1386207323999200730205447

[5] Petersen, E.; Hui, D.; Hamer, D. H.; Blumberg, L.; Madoff, L. C.; Pollack, M.; Lee, S. S.; McLellan, S.; Memish, Z.; Praharaj, I., Li Wenliang, a Face to the Frontline Healthcare Worker. The First Doctor to Notify the Emergence of the SARS-CoV-2,(COVID-19), Outbreak. *Int J Infect Dis.* **2020**, *93*, 205-207, DOI: https://doi.org/10.1016/j.ijid.2020.02.052.

[6] Poutanen, S. M.; Low, D. E.; Henry, B.; Finkelstein, S.; Rose, D.; Green, K.; Tellier, R.; Draker, R.; Adachi, D.; Ayers, M., Identification of Severe Acute Respiratory Syndrome in Canada. *N. Engl. J. Med* **2003**, *348* (20), 1995-2005, DOI: https://doi.org/10.1056/NEJMoa030634.

[7] Yamari, I.; Abchir, O.; Nour, H.; El Kouali, M.; Chtita, S., Identification of new dihydrophenanthrene derivatives as promising anti-SARS-CoV-2 drugs through in silico investigations, *Main Group Chem.*, **2022**, 1-16. https://doi.org/10.3233/MGC-220127.

[8] Chtita, S. ; Fouedjou, R. T., Belaidi, S., *et al. In silico* investigation of phytoconstituents from Cameroonian medicinal plants towards COVID-19 treatment. *Struct Chem.* **2022**, *33*, 1799-1813. https://doi.org/10.1007/s11224-022-01939-7.

[9] Belhassan, A.; Chtita, S.; Zaki, H.; Lakhlifi, T.; Bouachrine, M., Molecular docking analysis of N-substituted Oseltamivir derivatives with the SARS-CoV-2 main protease. *Bioinformation*. **2020**, *16* (5), 404-410. https://doi.org/10.6026/97320630016404.

[10] Belhassan, A.; Chtita, S.; Zaki, H.; Alaqarbeh, M.; Alsakhen, N.; Almohtaseb, F.; Lakhlifi, T.; Bouachrine, M., *In silico* detection of potential inhibitors from vitamins and their derivatives compounds against SARS-CoV-2 main protease by using molecular docking, molecular dynamic simulation and ADMET profiling, *J. Mol. Struct.*, **2022**, *1258*, 132652. https://doi.org/10.1016/j.molstruc.2022.132652.

[11] Ouassaf, M.; Belaidi, S.; Al Mogren, M. M.; Chtita, S.; Khan, S. U.; Htar, T. T., Combined docking methods and molecular dynamics to identify effective antiviral 2, 5-diaminobenzophenonederivatives against SARS-CoV-2, *Journal of King Saud University-Science*, **2021**, *33* (2), 101352. https://doi.org/10.1016/j.jksus.2021.101352.

[12] Chtita, S.; Belaidi, S.; Abul Qais, F.; Ouassaf, M.; AlMogren, M. M.; Al-Zahrani, A. A.; Bakhouch, M.; Belhassan, A.; Zaki, H.; Bouachrine, M.; Lakhlifi, T., Unsymmetrical aromatic disulfides as SARS-CoV-2

Mpro inhibitors: Molecular docking, molecular dynamics, and ADME scoring investigations, *Journal of King Saud University -Science*, **2022**, *34* (7), 102226. https://doi.org/10.1016/j.jksus.2022.102226.

[13] Fouedjou, R. T.; Daoui, O.; Nour, H.; Ayoub, M.; Fogang, H. P. D.; Siddique, F.; Elkhattabi, S.; Bakhouch, M.; Belaidi, S.; Chtita, S., *In Silico* Approach for Designing Novel SARS-CoV-2 Inhibitors from Medicinal Plants, *Phys. Chem. Res.*, **2023**, *11* (3), 589-604. https://doi.org/10.22036/PCR.2022.349693.2138.

[14] Yamari, I.; Abchir, O.; Mali, S. N.; Errougui, A.; Talbi, M.; El Kouali, M.; Chtita, S., The anti-SARS-CoV-2 activity of novel 9,10-dihydrophenanthrene derivatives: an insight into molecular docking, ADMET analysis, and molecular dynamics simulation, *Scientific African*, **2023**, *21*, e01754. https://doi.org/10.1016/j.sciaf.2023.e01754

[15] Gan, X.; Wang, Z.; Hu, D., Synthesis of Novel Antiviral Ferulic Acid-Eugenol and Isoeugenol Hybrids Using Various Link Reactions. *J. Agric. Food Chem.* **2021**, *69* (46), 13724-13733, DOI : https://doi.org/10.1021/acs.jafc.1c05521.

[16] Truzzi, F.; Whittaker, A.; D'Amen, E.; Tibaldi, C.; Abate, A.; Valerii, M. C.; Dinelli, G., Wheat Germ Spermidine and Clove Eugenol in Combination Stimulate Autophagy In Vitro Showing Potential in Supporting the Immune System against Viral Infections. *Molecules* **2022**, *27* (11), 3425, DOI: https://doi.org/10.3390/molecules27113425.

[17] Paidi, R. K.; Jana, M.; Raha, S., *et al.* Eugenol, a Component of Holy Basil (Tulsi) and Common Spice Clove, Inhibits the Interaction Between SARS-CoV-2 Spike S1 and ACE2 to Induce Therapeutic Responses. *J. NeuroImmune Pharmacol.* **2021**, *16*, 743-755, DOI: https://doi.org/10.1007/s11481-021-10028-1.

[18] Liu, Y.; Xu, S.; Bian, H.; Qian, Y.; Li, H.; Shu, S.; Chen, J.; Cao, X.; Gu, Y.; Jin, J., Xingnaojing Ameliorates Synaptic Plasticity and Memory Deficits in an Aβ1-42 Induced Mouse Model of Alzheimer's Disease. *J. Pharm. Sci.* **2020**, *143* (4), 245-254, DOI: 10.1016/j.jphs.2020.05.002.

[19] Abdou, A.; Idouaarame, S.; Salah, M.; Nor, N.; Zahm, S.; El Makssoudi, A.; Mazoir, N.; Benharref, A.; Dari, A.; Eddine, J. J.; Blaghen, M.; Dakir, M., Phytochemical Study: Molecular Docking of Eugenol Derivatives as Antioxidant and Antimicrobial Agents. *Lett. Org. Chem.* **2022**, *19* (9), 774-783, DOI: https://doi.org/10.2174/1570178619666220111112125

[20] da Silva, F. F. M.; Monte, F. J. Q.; de Lemos, T. L. G.; do Nascimento, P. G. G.; de Medeiros Costa, A. K.; de Paiva, L. M. M., Eugenol Derivatives: Synthesis, Characterization, and Evaluation of Antibacterial and Antioxidant Activities. *Chem. Cent. J.* **2018**, *12* (1), 34, DOI: https://doi.org/10.1186/s13065-018-0407-4.

[21] Coelho, C. M.; Santos, T. dos; Freitas, P. G.; Nunes, J. B.; Marques, M. J.; Padovani, C. G. D.; Júdice, W. A. S.; Camps, I.; Silveira, N. J. F. da; Carvalho, D. T.; Veloso, M. P., Design, Synthesis, Biological Evaluation and Molecular Modeling Studies of Novel Eugenol Esters as Leishmanicidal Agents. *J. Braz. Chem. Soc.* **2018**, *29*, 715-728, DOI: https://doi.org/10.21577/0103-5053.20170192.

[22] Hipólito, T. M. M.; Bastos, G. T. L.; Barbosa, T. W. L.; de Souza, T. B.; Coelho, L. F. L.; Dias, A. L. T.; Rodríguez, I. C.; dos Santos, M. H.; Dias, D. F.; Franco, L. L.; Carvalho, D. T., Synthesis, Activity, and Docking Studies of Eugenol-Based Glucosides as New Agents against Candida Sp. *Chem. Biol. Drug. Des.* **2018**, *92* (2), 1514-1524, DOI: https://doi.org/10.1111/cbdd.13318.

[23] de Souza, T. B.; de Oliveira Brito, K. M.; Silva, N. C.; Rocha, R. P.; de Sousa, G. F.; Duarte, L. P.; Coelho, L. F. L.; Dias, A. L. T.; Veloso, M. P.; Carvalho, D. T.; Dias, D. F., New Eugenol Glucoside-Based Derivative Shows Fungistatic and Fungicidal Activity against Opportunistic Candida Glabrata. *Chem. Biol. Drug. Des.* **2016**, *87* (1), 83-90, DOI :https://doi.org/10.1111/cbdd.12625.

[24] Martins, R. M.; Farias, M. D.; Nedel, F.; de Pereira, C. M. P.; Lencina, C.; Lund, R. G., Antimicrobial and Cytotoxic Evaluation of Eugenol Derivatives. *Med Chem Res* **2016**, *25* (10), 2360-2367; DOI: https://doi.org/10.1007/s00044-016-1682-z.

[25] Carvalho, L. I. S. de; Alvarenga, D. J.; Carmo, L. C. F. do; Oliveira, L. G. de; Silva, N. C.; Dias, A. L. T.; Coelho, L. F. L.; Souza, T. B. de; Dias, D. F.; Carvalho, D. T., Antifungal Activity of New Eugenol-

Benzoxazole Hybrids against *Candida* Spp. *J. Chem.* **2017**, *2017*, e5207439, DOI: https://doi.org/10.1155/2017/5207439.

[26] Abdou, A.; Elmakssoudi, A.; El Amrani, A.; JamalEddine, J.; Dakir, M., Recent Advances in Chemical Reactivity and Biological Activities of Eugenol Derivatives. *Med. Chem. Res.* **2021**, *30* (5), 1011-1030, DOI: https://doi.org/10.1007/s00044-021-02712-x.

[27] Topal, F.; Gulcin, I.; Dastan, A.; Guney, M., Novel Eugenol Derivatives: Potent Acetylcholinesterase and Carbonic Anhydrase Inhibitors. *Int. J. Biol. Macromol.* **2017**, *94*, 845-851, DOI: https://doi.org/10.1016/j.ijbiomac.2016.10.096.

[28] Devkate, S.; Burungale, A.; Jadhav, S.; Pise, A.; Gawde, R., Synthesis of γ-Lactones by Nucleophilic Addition of Carboxylic Acid Enediolates to Epoxides. *J. Emerg. Technol. Innov. Res.* **2019**, *6* (2) 738-742, DOI: https://doi.org/10.1729/Journal.19845.

[29] Melean, L. G.; Rodriguez, M.; Romero, M.; Alvarado, M. L.; Rosales, M.; Baricelli, P. J., Biphasic Hydroformylation of Substituted Allylbenzenes with Water-Soluble Rhodium or Ruthenium Complexes. *Appl. Catal.* **2011**, *394* (1), 117-123, DOI: https://doi.org/10.1016/j.apcata.2010.12.037.

[30] Lenardão, E. J.; Jacob, R. G.; Mesquita, K. D.; Lara, R. G.; Webber, R.; Martinez, D. M.; Savegnago, L.; Mendes, S. R.; Alves, D.; Perin, G., Glycerol as a Promoting and Recyclable Medium for Catalyst-Free Synthesis of Linear Thioethers: New Antioxidants from Eugenol. *GCLR.* **2013**, *6* (4), 269-276, DOI: https://doi.org/10.1080/17518253.2013.811298.

[31] Genç Bilgiçli, H.; Kestane, A.; Taslimi, P.; Karabay, O.; Bytyqi-Damoni, A.; Zengin, M.; Gulçin, İ., Novel Eugenol Bearing Oxypropanolamines: Synthesis, Characterization, Antibacterial, Antidiabetic, and Anticholinergic Potentials. *Bioorg. Chem.* **2019**, *88*, 102931, DOI: https://doi.org/10.1016/j.bioorg.2019.102931.

[32] Ahmad A., *et al.* Synergistic Interactions of Eugenol-Tosylate and Its Congeners with Fluconazole against Candida Albicans. *PLoS. One* **2015**, *10* (12) 1-19, DOI: https://doi.org/10.1371/journal.pone.0145053.

[33] Ginting, M., Synthesis of 2-(4-Allyl-2-Methoxy Phenoxy)-N,N-Bis(2- Hydroxyethyl) Acetamide from the Transformation of Eugenol Isolated from Clove Oil. *JCNaR* **2019**, *1* (1), 31-39, DOI: https://doi.org/10.32734/jcnar.v1i1.832.

[34] Hidalgo, M. E.; De la Rosa, C.; Carrasco, H.; Cardona, W.; Gallardo, C.; Espinoza, L. Antioxidant Capacity of Eugenol Derivatives. *Quím. Nova* **2009**, *32*, 1467-1470, DOI: https://doi.org/10.1590/S0100-40422009000600020.

[35] Olea, A. F.; Bravo, A.; Martínez, R.; Thomas, M.; Sedan, C.; Espinoza, L.; Zambrano, E.; Carvajal, D.; Silva-Moreno, E.; Carrasco, H., Antifungal Activity of Eugenol Derivatives against Botrytis Cinerea. *Molecules* **2019**, *24* (7), 1239, DOI: https://doi.org/10.3390/molecules24071239.

[36] Elgendy, E. M.; Khayyat, S. A., Oxidation Reactions of Some Natural Volatile Aromatic Compounds: Anethole and Eugenol. *Russ. J. Org. Chem.* **2008**, *44* (6), 823-829, DOI: https://doi.org/10.1134/S1070428008060079.

[37] Lauro, F.; Cedillo, D.; Marcela, R., Design and Synthesis of a Diazabicyclo-Naphthalen-Oxiranyl-Methanone Derivative. Theoretical Analysis of Their Interaction with Cytochrome P450-17A1. *Chem. Methodol* **2019**, *3*, 194-210, DOI: https://doi.org/10.22034/chemm.2018.147492.1083.

[38] Sudarma, I. M., *et al.* Chemical Transformation of Eugenol Isolated from Leaves of Syzygium Aromaticum to Its New Isothiocyanate Derivatives. *J. Nat. Prod.* **2015**, *8*, 27-32. DOI: ?

[39] Rudyanto, M.; Ekowati, J.; Widiandani, T.; Honda, T., Synthesis and Brine Shrimp Lethality Test of Some Benzoxazine and Aminomethyl Derivatives of Eugenol. *Int. J. Pharm. Pharmaceut. Sci.* **2014**, *6*, 96-98. DOI: ?

[40] Li, Y.; Luo, F.; Cheng, C. Preparation of Eugenol-Based Polyurethane. *IOP Conf. Ser.: Mater. Sci. Eng.* **2018**, *322* (2), 022030. DOI: https://doi.org/10.1088/1757-899X/322/2/022030.

[41] Sharma, S.; Kumar, P.; Chandra, R., Chapter 7-Applications of BIOVIA Materials Studio, LAMMPS, and GROMACS in Various Fields of Science and Engineering. *Molecular Dynamics Simulation of Nanocomposites Using BIOVIA Materials Studio, Lammps and Gromacs,* **2019**, 329-341, DOI:

https://doi.org/10.1016/B978-0-12-816954-4.00007-3.

[42] Pires, D. E. V.; Blundell, T. L.; Ascher, D. B., PkCSM: Predicting Small-Molecule Pharmacokinetic and Toxicity Properties Using Graph-Based Signatures. *J. Med. Chem.* **2015**, *58* (9), 4066-4072, DOI: https://doi.org/10.1021/acs.jmedchem.5b00104.

[43] Trott, O.; Olson, A. J. AutoDock Vina: Improving the Speed and Accuracy of Docking with a New Scoring Function, Efficient Optimization, and Multithreading. *J. Comput. Chem.* **2010**, *31* (2), 455-461, DOI : https://doi.org/10.1002/jcc.21334.

[44] Abraham, M. J.; Murtola, T.; Schulz, R.; Páll, S.; Smith, J. C.; Hess, B.; Lindahl, E., GROMACS: High Performance Molecular Simulations through Multi-Level Parallelism from Laptops to Supercomputers. *SoftwareX* **2015**, *1-2*, 19-25, DOI: https://doi.org/10.1016/j.softx.2015.06.001.

[45] Bjelkmar, P.; Larsson, P.; Cuendet, M. A.; Hess, B.; Lindahl, E., Implementation of the CHARMM Force Field in GROMACS: Analysis of Protein Stability Effects from Correction Maps, Virtual Interaction Sites, and Water Models. *J. Chem. Theory Comput.* **2010**, *6* (2), 459-466, DOI: https://doi.org/10.1021/ct900549r.

[46] Vincent, Z. A., CM; Aurélien, G.; Olivier, M., SwissParam: A Fast Force Field Generation Tool for Small 150 Organic Molecules. *J. Comput. Chem. 32*, 2359-2368, DOI: https://doi.org/10.1002/jcc.21816.

[47] Parrinello, M.; Rahman, A., Polymorphic Transítions in Single Crystals: A New Molecular Dynamics Method Polymorphic Transítions in Single Crystals: A New Molecular Dynamics Method. *J. Appl. Phys.* **2002**, *12* (52), 7182, DOI: https://doi.org/10.1063/1.328693.

[48] Lipinski, C. A.; Lombardo, F.; Dominy, B. W.; Feeney, P. J., Experimental and Computational Approaches to Estimate Solubility and Permeability in Drug Discovery and Development Settings. *Adv. Drug Deliv. Rev.* **2001**, *46* (1), 3-26, DOI: https://doi.org/10.1016/s0169-409x(00)00129-0.

[49] Veber, D. F.; Johnson, S. R.; Cheng, R. Y. H.; Smith, B. R.; Ward, K. W.; Kopple, K. D., *J. Med. Chem.* **2002**, *45*, 2615-2623, DOI: https://doi.org/10.1021/jm020017n.

[50] Shekhawat, P.; Pokharkar, V., Understanding Peroral Absorption: Regulatory Aspects and Contemporary Approaches to Tackling Solubility and Permeability Hurdles. *Acta Pharmaceutica Sinica B* **2017**, *7* (3), 260-280. DOI: https://doi.org/10.1016/j.apsb.2016.09.005.